RADIATION (UV-IR) MEASUREMENTS IN THE TRIAM-1 TOKAMAK

Nakamura, Kazuo
Research Institute for Applied Mechanics, Kyushu University : Research Associate

Nakamura, Yukio
Research Institute for Applied Mechanics, Kyushu University : Research Associate

Hiraki, Naoji
Research Institute for Applied Mechanics, Kyushu University : Research Associate

Itoh, Satoshi
Research Institute for Applied Mechanics, Kyushu University : Professor

https://doi.org/10.5109/6777126

出版情報：Reports of Research Institute for Applied Mechanics. 29 (91), pp.61-77, 1981-07. 九州大学応用力学研究所

Reports of Research Institute for Applied Mechanics
Vol. XXIX, No. 91, 1981

RADIATION (UV-IR) MEASUREMENTS IN THE TRIAM-1 TOKAMAK

By Kazuo NAKAMURA*, Yukio NAKAMURA*, Naoji HIRAKI* and Satoshi ITOH**

Scaling law is presented that the ratio P_R/P_I (P_R: radiation loss, P_I: input power) is proportional to the parameter $a^{3/2}/R$ (a: minor radius, R: major radius). And the discussion is presented about the design of the apparatus for measuring the radiation (ultraviolet to infrared) from the TRIAM-1 tokamak plasma.

Key words: Scaling law, Radiation loss, TRIAM-1 tokamak

1. Introduction

It is necessary for thermonuclear fusion reactor that the ion temperature T_i is greater than 10 keV and product of the ion density n and the energy confinement time τ is greater than 10^{14} cm^{-3} sec (Lawson criterion). In the TRIAM-1 tokamak[1] we endeavor to increase T_i by turbulent heating[2] (Appendix A) and to increase n and so τ by high magnetic field and gas puffing.

Even if much gas is puffed into the tokamak plasma, n increases no longer unless the current density increases. The reason is as follows[3]: The radiation cooling of the plasma edge occurs when much gas is puffed, the current density profile is shrinked and the plasma is apart from the metal limiter (and the stabilization effect is lost), and thermal instability, low-m-number MHD-instability, major current disruption, and so on occur. In this report we propose the scaling law concerning radiation loss in relation to this limit.

We designed the apparatus for measuring the radiation (ultra violet to infrared) in the TRIAM-1 tokamak with high temporal and spatial resolution. In this report we discuss also about the design.

* Research Associate, Research Institute for Applied Mechanics, Kyushu University.
** Professor, Research Institute for Applied Mechanics, Kyushu University.

2. Energy balance

2.1. The ratio of radiation loss to input power

The ratio of the radiation loss P_R to the input power P_I in tokamaks is plotted in Fig. 1. The figure shows that the ratio P_R/P_I is proportional to the parameter $a^{3/2}/R$. Since the aspect ratio of tokamak plasmas is nearly constant to be 3 to 6 as shown in Fig. 2, the ratio P_R/P_I is proportional to $a^{1/2}$. Namely the fraction of the radiation increases as the tokamak plasma becomes larger.

This proportionality is explained as follows. Since the maximum average density $(\overline{n_e})_{max}$ is considered to be limited by the radiation cooling of the plasma edge, the following equation is lead[3], by assuming the $(\overline{n_e})_{max}$-value is obtained for $P_R/P_I=F\,(<1)$,

$$(\overline{n_e})_{max} = \left\{\frac{0.1F}{\alpha_R \xi T_e}\right\}^{1/2} \frac{I_p}{\pi a^2}, \tag{1}$$

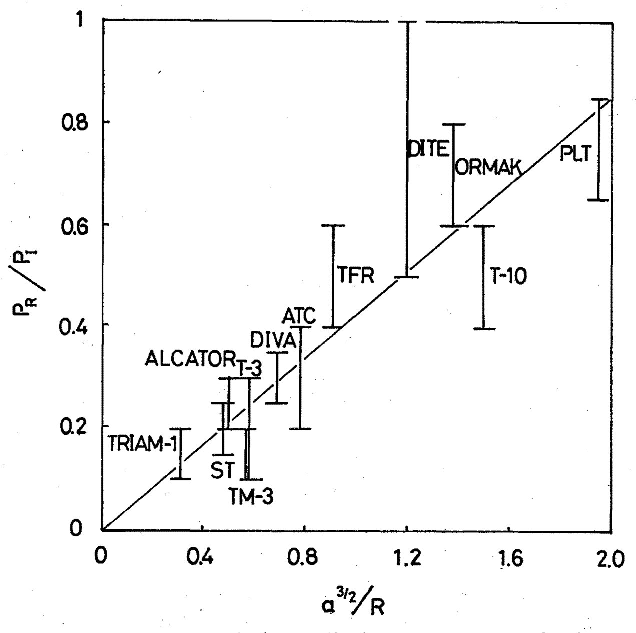

Fig. 1. The ratio of the radiation loss P_R to the input power P_I in tokamaks. Minor radius a and major radius R are in cm. The various tokamaks are referenced as follows: ST, TM-3, T-3, ATC, TFR, DITE, ORMAK, T-10 and PLT are referenced from ref. 6, ALCATOR from ref. 7 and DIVA from ref. 8. The datum in TRIAM-1 is the value expected by this scaling law.

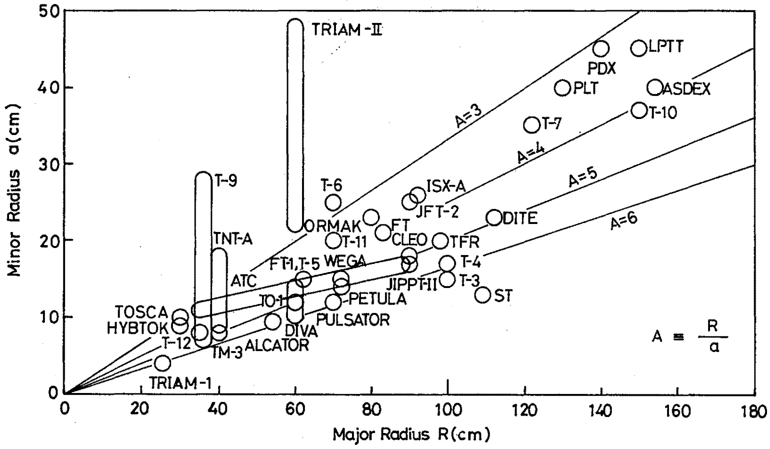

Fig. 2. The aspect ratio A of small-scale and medium-scale tokamak plasmas. The long circles indicate tokamak plasmas of non-circular cross-section.

where α_R and ξ are numerical constants, $\overline{T_e}$ and I_P are average electron temperature and plasma current, respectively. On the other hand $(\overline{n_e})_{max}$ is represented experimentally by the following equation[4],

$$(\overline{n_e})_{max} = \frac{10^{13}}{0.9} \frac{B_T}{R} (\mathrm{cm}^{-3}), \tag{2}$$

where B_T is toroidal field in Tesla and R in meter. Since safety factor $q_a = (a/R)\{B_T/(\mu_0 I_P/2\pi a)\}$ is nearly constant, both eqs. (1) and (2) mean the same result that $(\overline{n_e})_{max}$ is proportional to the current density. Accordingly,

$$F = \frac{\alpha_R \xi \overline{T_e}}{0.1} \left\{ \frac{10^{13}}{0.9} \frac{B_T}{R} \frac{\pi a^2}{I_P} \right\}^2 = \frac{\alpha_R \xi \overline{T_e}}{0.1} \left\{ \frac{10^{13}}{0.9} \frac{\mu_0 q_a}{2} \right\}^2 \propto \overline{T_e} \tag{3}$$

This result and Fig. 1 lead to

$$\overline{T_e} \propto a^{1/2} \tag{4}$$

i.e. the larger the tokamak plasma is, the higher the temperature is. The proporiety of this result verifies that $(\overline{n_e})_{max}$ is limited by the radiation cooling of the plasma edge.

2.2. Energy balance in the TRIAM-1 tokamak

According to the scaling law shown in Fig. 1, about 15% of the input power is expected to be lost by the radiation in the TRIAM-1 tokamak. In Fig. 3 the value of the charge-exchange loss from ions is estimated from the experimental result by the neutral energy analyzer[5]. The power transported from electrons to ions is estimated by assuming the

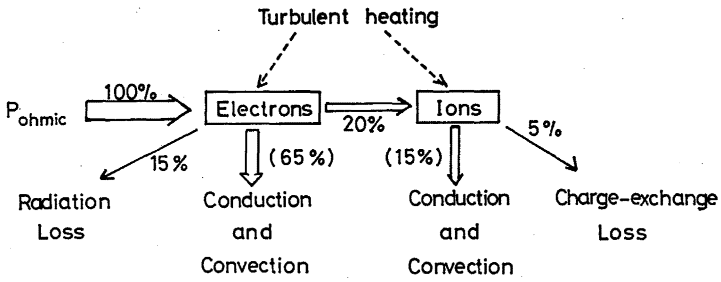

Fig. 3. The energy balance in the TRIAM-1 tokamak. The percentage in bracket is not measured but calculated: 20% is estimated from the classical theory of equipartition and 65% and 15% are estimated as the residual loss.

Table I. The specification of S1337-16BQ.

The size of sensitive surface	1.1×5.9 mm
The effective area of the above	$5.8\ \mathrm{mm}^2$
Noise equivalent power	$NEP = 6\times10^{-15}\ \mathrm{W/Hz}^{1/2}$
Detectivity	$D^* = 3\times10^{13}\ \mathrm{cmHz}^{1/2}/\mathrm{W}$
Dark current	$I_d = 25$ pA
Parallel resistance	$R_{sh} = 2\ \mathrm{G}\Omega$
Conjunction capacity	$C_j = 65$ pF
Inverse voltage	$V_R = 5$ V
Rise time (for $V_R = 0$ V and $R_f = 1\ \mathrm{k}\Omega$)	$t_r = 0.2\ \mu\mathrm{s}$
Temperature	-10 to $+60$(°C)

classical Coulomb interaction The fraction of the conduction and convection loss from electrons and ions are estimated as the residual loss, since they are unable to be measured directly.

Figure 4 shows the radial profile $P_R(r)$ of the radiation due to oxygen impurity in case of the profiles of electron density $n_e(r)$ and electron temperature $T_e(r)$ shown in the same figure. The profile $P_R(z)$ is the profile integrated along the horizontal sight-line.

3. Apparatus for measuring radiation

In order to study the mechanism of density limit due to radiation cooling, the high temporal and spatial resolution of radiation measurement is necessary, since the radiation loss may concentrate in the local narrow region and unfavorable instabilities may occur rapidly.

The energy range of radiation loss from the tokamak plasma is shown in Fig. 5. The sensitivity of the detector adopted (S1337-16BQ) is shown in Fig. 6 and the specification is shown in Table I. The sig-

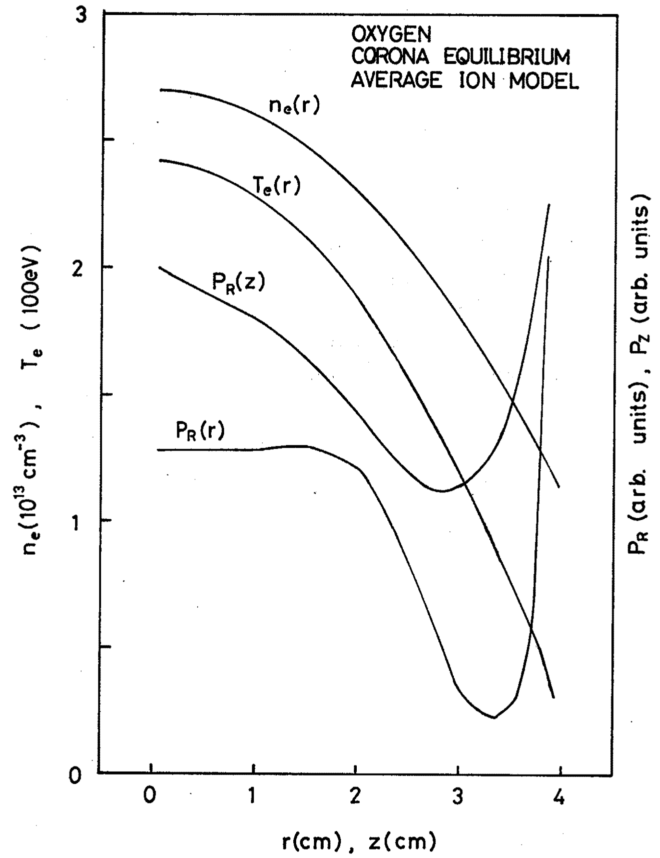

Fig. 4. The expected radial profile $P_R(r)$ of the radiation loss in case of the typical profiles of electron density $n_e(r)$ and electron temperature $T_e(r)$. The profile $P_R(z)$ is the profile Abel-inverted from the profile $P_R(r)$. The value $P_R(r)$ is estimated by the average ion model[9] assuming corona equilibrium.

nal converted from photon flux to charge current by the detector is transformed to voltage by the electric circuit shown in Fig. 7 and the voltage is traced on the oscilloscope.

Figure 8 shows the side view of the TRIAM-1 tokamak and the apparatus for measuring the radiation. The detectors are able to approach the plasma to measure the radiation profile with high spatial resolution. When the measurement is not carried, the gate valve GV-1 is able to separate the TRIAM-1 vacuum chamber and the apparatus. The collimator limiting the solid angle observed by the detector consists of the five

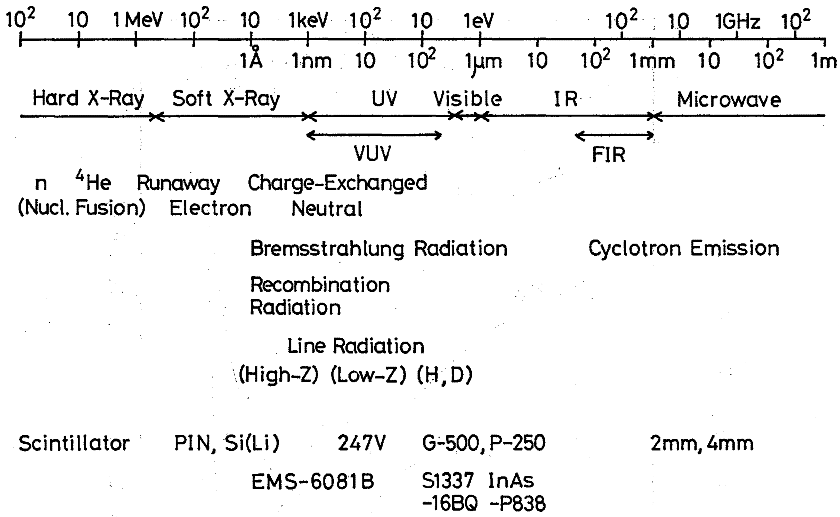

Fig. 5. The energy range and the detectors of the particles and radiation in tokamaks.

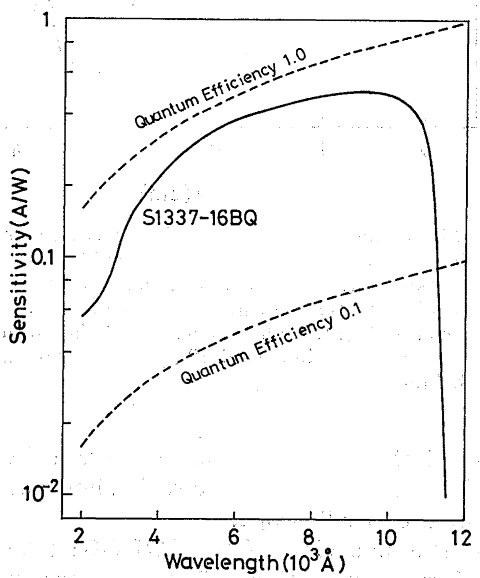

Fig. 6. The sensitivity of S1337-16BQ. The cut-off on the long-wavelength side is determined by the band gap of silicon $F_g = 1.12$ eV. The cut-off on the short-wavelength side is determined by the thickness of P-layer.

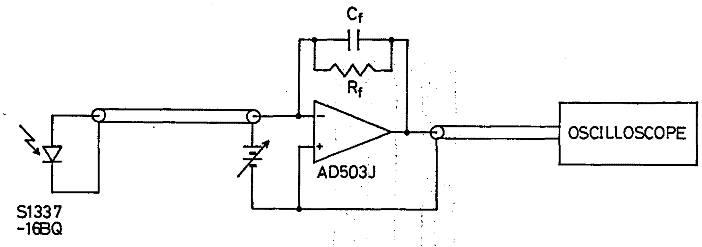

Fig. 7. The electric circuit for transformation of current-type signal of S1337-16BQ to voltage-type signal traced on the oscilloscope. The damping capacity C_f is mainly to prevent the self-oscillation and is a few pico-farad. The feedback resistance R_f is selected so as to be smaller than the parallel resistance R_{sh} of S1337-16BQ. The bias current of FET-input-type OP-amp AD503J is less than a few ten pico-ampere. The bias voltage is in order to make larger the response speed and the upper limit of linearity of incident photon flux vs. output current.

parallel slits (Fig. 9), which prevent the stray radiation due to reflection of the radiation on the internal surface of the collimator.

4. Conclusion

We presented the scaling law: The ratio P_R/P_I is proportional to the parameter $a^{3/2}/R$, where P_R, P_I, a and R are the radiation loss, input power, minor radius and major radius, respectively. This scaling law was lead from the assumption that the average density $\overline{n_e}$ can be made higher until the ratio P_R/P_I reaches some value.

And we presented the design of the apparatus for measuring the radiation loss with high temporal and spatial resolution in order to observe the radiation loss associated with the phenomena limiting the maximum average density $(\overline{n_e})_{max}$ such as thermal instability, low-m-number MHD-instability and major current disruption.

References

1) Hiraki, N., Itoh, S., Kawai, Y., Toi, K., Nakamura, K. and Mitarai, O.: *Confinement of Ohmically Heated Plasmas and Turbulent Heating in High-Magnetic-Field Tokamak TRIAM-1*, Reports of Research Institute for Applied Mechanics **27** No. 85 (1979) 85.

2) Toi, K., Hiraki, N., Nakamura, K., Mitarai, O., Kawai, Y. and Itoh, S.: *Observation of Bulk-Ion Heating in a Tokamak Plasma by Application of Positive and Negative Current Pulses in TRIAM-1*, Nucl. Fusion **20** No. 9 (1980) 1169.

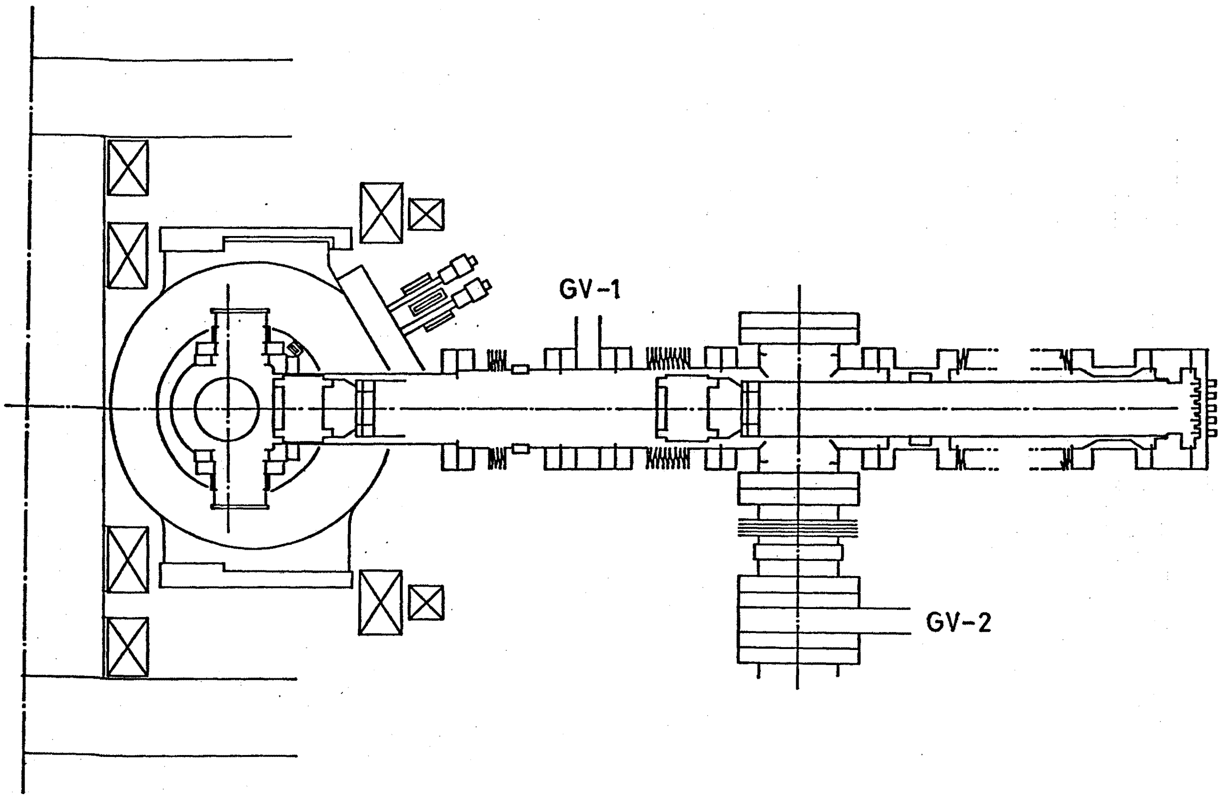

Fig. 8. The schematic diagram of the TRIAM-1 tokamak and the apparatus for measuring the radiation loss.

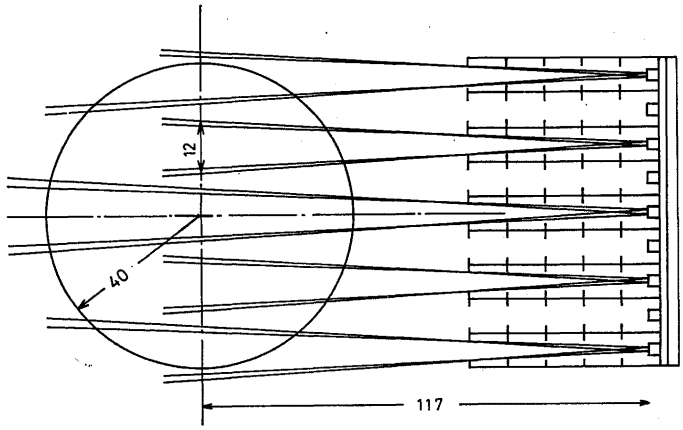

Fig. 9. The structure of the collimator which is designed to obtain the spatial resolution of 12 mm even if the internal surface is not blackened.

3) Gibson, A.: *Radiation Limits to Tokamak Operation*, Nucl. Fusion **16** No. 3 (1976) 546.
4) Murakami, M., Callen, J. D. and Berry, L. A.: *Some Observations on Maximum Densities in Tokamak Experiments*, Nucl. Fusion **16** No. 2 (1976) 347.
5) Nakamura, K., Hiraki, N., Toi, K. and Itoh, S.: *Ion Temperature Measurement by Neutral Energy Analyzer in High-Field Tokamak TRIAM-1*, Reports of Research Institute for Applied Mechanics **27** No. 86 (1980) 125.
6) Edmonds, P. H. and England, A. C.: *Energy Loss to the Wall and Limiter in Normal ORMAK Discharges*, Nucl. Fusion **18** No. 1 (1978) 23.
7) Scaturro, L. S. and Pickrell, M. M.: *Bolometric Measurements and the Role of Radiation in ALCATOR Power Balance*, Nucl. Fusion **20** No. 5 (1980) 527.
8) Yamamoto, S., Maeda, H., Shimomura, Y., Odajima, K., Nagami, M., Kimura, H., Sengoku, S., Ohtsuka, H., Ueda, N., Funahashi, A., Matoba, T., Takeuchi, H., Takahashi, K., Kasai, S., Sugie, T., Shiho, M., Kawakami, T., Kumagai, K., Yamauchi, T., Shoji, T., Tokutake, T., Anno, K., Arai, T., Shibata, T., Hiratsuka, H., Tanaka, M., Tanaka, Y. and Kunieda, S.: *Reduction of Power Loss due to Heavy Impurities in DIVA*, Proc. 8th Eur. Conf. on Contr. Fusion and Plasma Phys. (Prague, 1977) Vol. I, 33.
9) Jensen, R. V., Post, D. E., Grasberger, W. H., Tarter, C. B. and Lokke, W. A.: *Calculations of Impurity Radiation and its Effects on Tokamak Experiments*, Nucl. Fusion **17** No. 6 (1977) 1187.
10) Zakharov, L. E.: *Numerical Methods for Solving Some Problems of the Theory of Plasma Equilibrium in Toroidal Configurations*, Nucl. Fusion **13** No. 4 (1973) 595.
11) Kobayashi, T., Tamura, S. and Tani, K.: *Optimum Design of Ohmic Heating Field Coils for an Air-Core System and Equilibrium Field Coils of a Large Scale Fusion Device*, Report of Japan Atomic Energy Research Institute, JAERI-5898 (1974).

(Received April 30, 1981)

Appendix A. Design of Turbulent Heating Coil in TRIAM-1

The toroidal electric field for turbulent heating is made by flowing current in 4 windings in the toroidal direction. We determined the configuration of the 4 windings and the ratio of each current in them, taking into account the effect of the stray magnetic field made by them, i.e. it has been taken into account that the bad-direction stray vertical field gets out the plasma and the good-direction stray vertical field holds the plasma at the center, even if the plasma is heated by the turbulent heating.

In order to make the stray field zero, hollow-donut shell had better be used as the coil. But it has to have many holes for the diagnostic apparatusses to be applied to the plasma and so play the role as the source of stray field rather than the perfect conductor. Therefore in TRIAM-1, the discrete shell, i.e. the windings have been adopted. The process of changes from the perfect shell to the windings is especially discussed in this appendix.

A. 1 Surface current density distribution of superconductor

In this section we consider the infinite number of windings, i.e. perfect conductive shell.

At first we determine the surface current density distribution so as not to make the stray field in the vacuum chamber in case of the circular cross-section. This corresponds the current density distribution of superconductor, since there is no magnetic field in it.

We have only to make the field on the boundary (on the surface) zero in order to make the field inside the boundary zero. As shown in Fig. A–1, we divide the surface into n parts of the same size and make the current flowing in the i-th part as I_i. In order that the field at the i-th part made by the currents at the other parts is zero[9),10)],

$$\begin{pmatrix} a_{11} & a_{12} & \cdots & a_{1n} \\ a_{21} & a_{22} & \cdots & a_{2n} \\ \cdots & \cdots & \cdots & \cdots \\ a_{n1} & a_{n2} & \cdots & a_{nn} \end{pmatrix} \begin{pmatrix} I_1 \\ I_2 \\ \vdots \\ I_n \end{pmatrix} = \begin{pmatrix} 0 \\ 0 \\ \vdots \\ 0 \end{pmatrix}, \tag{A-1}$$

$$a_{ii} = -\sum_{k \neq i} b_\tau(\mathrm{k}, \mathrm{i}) \Delta \ell_\mathrm{k}, \tag{A-2}$$

$$a_{ij} = b_\tau(\mathrm{i}, \mathrm{j}) \Delta \ell_\mathrm{j} \quad (\mathrm{i} \neq \mathrm{j}), \tag{A-3}$$

$$b_\tau(\mathrm{i}, \mathrm{j}) = B_z(r, z, \rho, \xi) \cos\theta_i - B_r(r, z, \rho, \xi) \sin\theta_i, \tag{A-4}$$

$$r = R + a\cos\theta_i, \tag{A-5}$$

$$z = a\sin\theta_i, \tag{A-6}$$

$$\rho = R + a\cos\theta_j, \tag{A-7}$$

$$\xi = a\sin\theta_j, \tag{A-8}$$

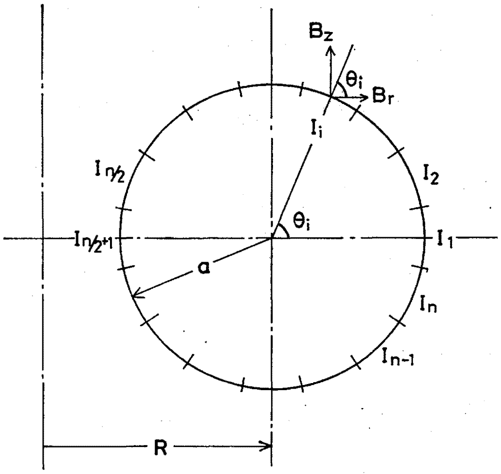

Fig. A-1. The schematic diagram for the calculation of the surface current density on the superconductor of circular cross-section.

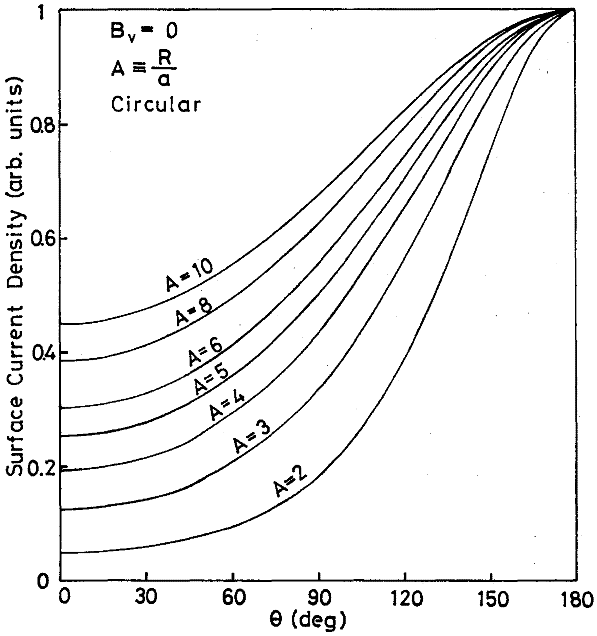

Fig. A-2. Dependence of surface current density of superconductor on the angle θ (defined as shown in Fig. A-1) with aspect ratio A as a parameter.

$$B_r(r, z, \rho, \xi) = \frac{\mu_0 I}{2\pi\sqrt{(r+\rho)^2+(z-\xi)^2}} \frac{z-\xi}{r}$$

$$\times\left\{-\mathrm{K}(k)+\frac{r^2+\rho^2+(z-\xi)^2}{(r-\rho)^2+(z-\xi)^2}\mathrm{E}(k)\right\}, \quad \text{(A-9)}$$

$$B_z(r, z, \rho, \xi) = \frac{\mu_0 I}{2\pi\sqrt{(r+\rho)^2+(z-\xi)^2}}$$

$$\times\left\{\mathrm{K}(k)-\frac{r^2-\rho^2+(z-\xi)^2}{(r-\rho)^2+(z-\xi)^2}\mathrm{E}(k)\right\}, \quad \text{(A-10)}$$

$$k^2 = \frac{4r\rho}{(r+\rho)^2+(z-\xi)^2}, \quad \text{(A-11)}$$

$$\theta_k = \frac{2\pi}{n}(k-1) \qquad (k = 1, 2, \cdots\cdots n,), \quad \text{(A-12)}$$

$$I = 1, \quad \text{(A-13)}$$

$$\Delta\ell_k = a\frac{2\pi}{n}, \quad \text{(A-14)}$$

$$\mu_0 = 4\pi\times10^{-7}. \quad \text{(A-15)}$$

Since the solution of this equation is not unique, we solve the following equation instead,

$$\begin{pmatrix} a_{21} & a_{22} & \cdots\cdots & a_{2n} \\ \cdots & \cdots & \cdots & \cdots \\ \cdots & \cdots & \cdots & \cdots \\ a_{n1} & a_{n2} & \cdots\cdots & a_{nn} \end{pmatrix} \begin{pmatrix} I_1 \\ I_2 \\ \vdots \\ I_n \end{pmatrix} = \begin{pmatrix} 0 \\ \vdots \\ \vdots \\ 0 \end{pmatrix}, \quad \text{(A-16)}$$

$$I_k = 1 \qquad (k = n/2+1) \quad (n\text{: even}). \quad \text{(A-17)}$$

The numerical solution is shown in Fig. A-2.

In case of the elliptic cross-section as shown in Fig. A-3, the abvoe equations change to be as follows:

$$b_r(i, j) = B_z(r, z, \rho, \xi)\cos\omega_i - B_r(r, z, \rho, \xi)\sin\omega_i, \quad \text{(A-18)}$$

$$\tan\omega_i = \frac{a}{b}\tan\theta_i \quad \text{(A-19)}$$

$$r = R+a\cos\theta_i \quad \text{(A-20)}$$

$$z = b\sin\theta_i \quad \text{(A-21)}$$

$$\rho = R+a\cos\theta_j \quad \text{(A-22)}$$

$$\xi = b\sin\theta_j \quad \text{(A-23)}$$

$$\Delta\ell_k = \sqrt{(a\cos\theta_k)^2+(b\sin\theta_k)^2}\,\frac{2\pi}{n} \quad \text{(A-24)}$$

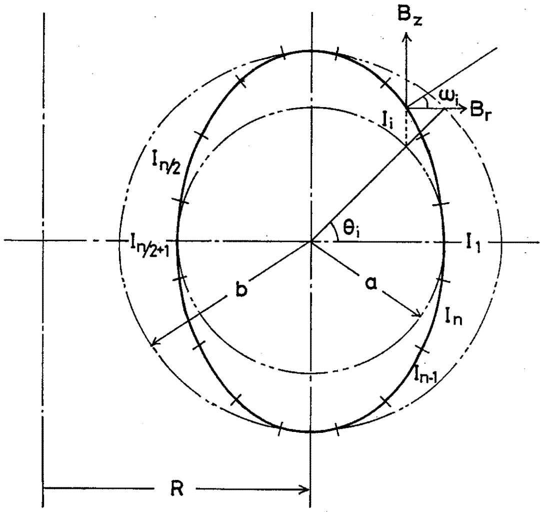

Fig. A-3. The schematic diagram for the calculation of the surface current density on the superconductor of elliptic cross-section.

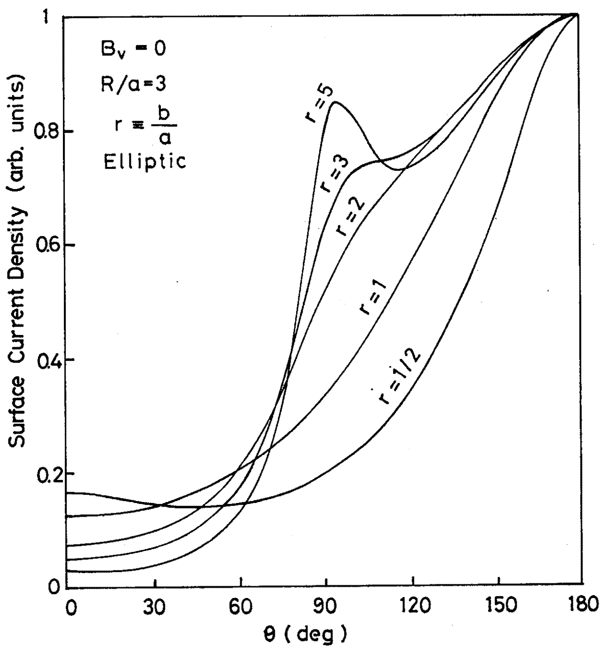

Fig. A-4. Dependence of surface current density of superconductor on the angle θ (defined as shown in Fig. A-3) with the ratio of height and width as a parameter.

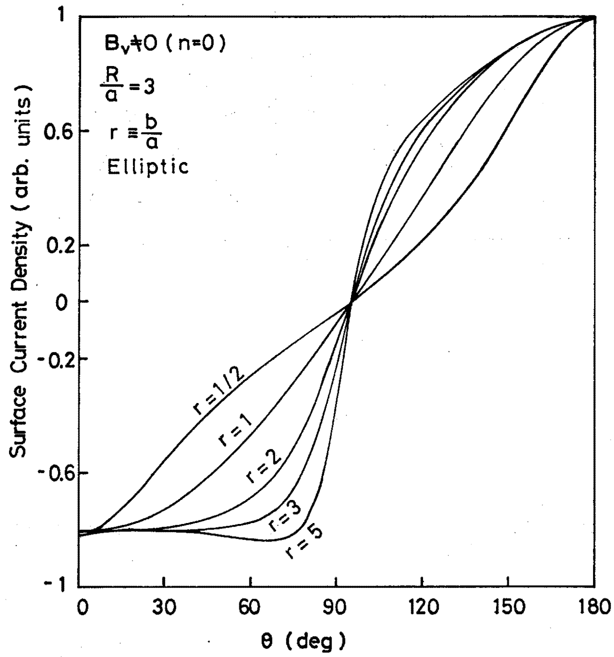

Fig. A-5. Surface current density in order to make the uniform vertical field in case of circular cross-section.

The numerical solution is shown in Fig. A-4.

In turbulent heating in tokamaks, we need to make the vertical field to hold the plasma at the center of the vacuum chamber, although we need to make the stray field zero. We have only to change the right hand side (=0) of eq. (A-16) to the necessary vertical field (=1), in order to obtain the necessary surface current density. The numerical result is shown in Fig. A-5 in case of circular cross-section and in Fig. A-6 in case of elliptic cross-section. Of course there is indefiniteness in the meaning that the sum of the above two results (i.e. Fig. A-2 and Fig. A-5, or Fig. A-4 and Fig. A-6) is also the solution.

A.2. Current ratio in the windings for turbulent heating

In this section we consider the distribution of the windings and their current ratio concretely in case of TRIAM-1 (the 1st Tokamak of Research Institute for Applied Mechanics).

With respect to the location of the windings for turbulent heating we cannot afford to search. In case of 6 windings the location is shown in Fig. A-7 and in case of 4 windings in Fig. A-8. Their current ratios

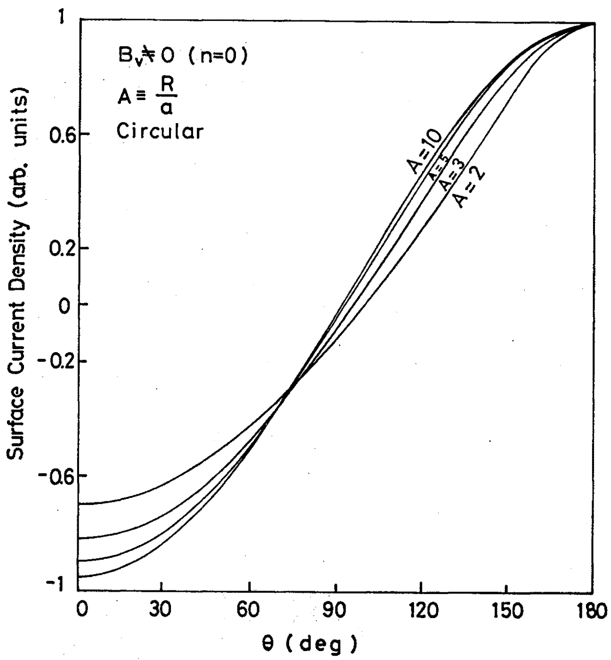

Fig. A-6. Surface current density in order to make the uniform vertical field in case of elliptic cross-section.

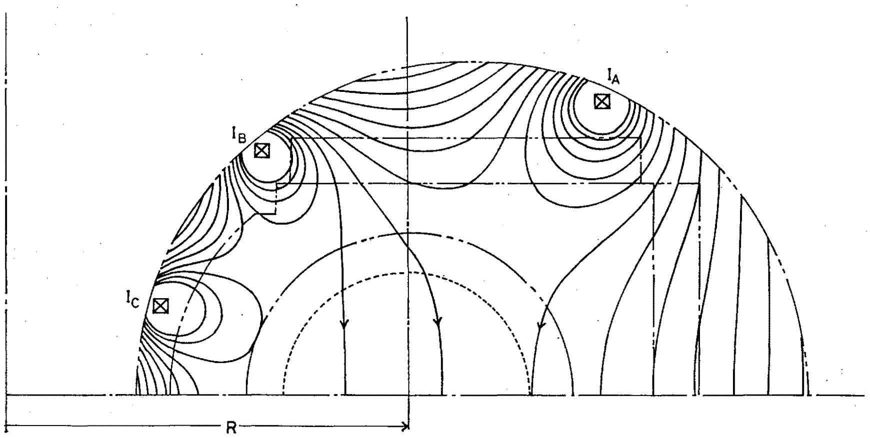

Fig. A-7. The location of upper 3 windings for turbulent heating and the flux surfaces in TRIAM-1: I_A=5 kA, I_B=9 kA and I_C=11 kA.

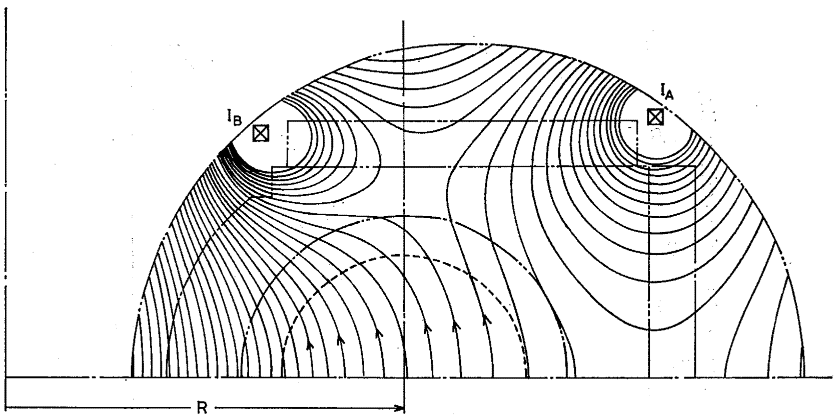

Fig. A-8. The location of upper 2 windings for turbulent heating and the flux surfaces in TRIAM-1: I_A=7.6 kA and I_B=17.4 kA.

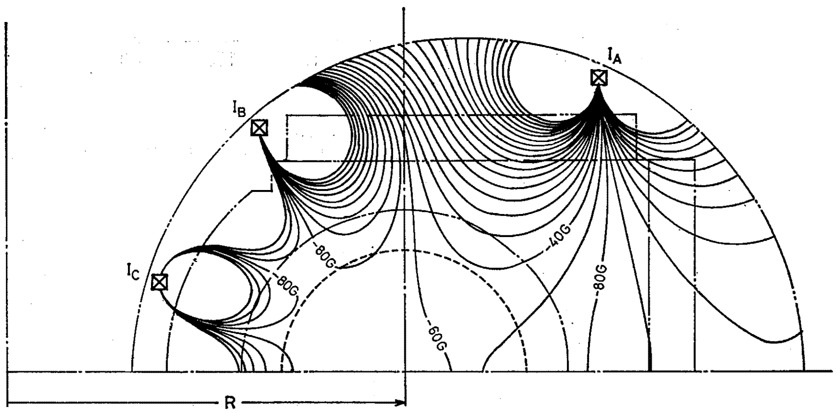

Fig. A-9. The contour lines of the vertical field in case of 6 windings. The values of I_A, I_B and I_C are the same as in Fig. A-7.

are determined so that the stray magnetic field in the plasma region is minimum in case of 6 windings and so that stray vertical field in the plasma region is optimum in case of 4 windings. The magnetic surfaces are shown in Fig. A-7 and A-8. The contour lines of the stray vertical field are shown in Fig. A-9 and A-10.

In case of 4 windings the vertical field in the plasma center is able to be changed by changing the current ratio as shown in Fig. A-11.

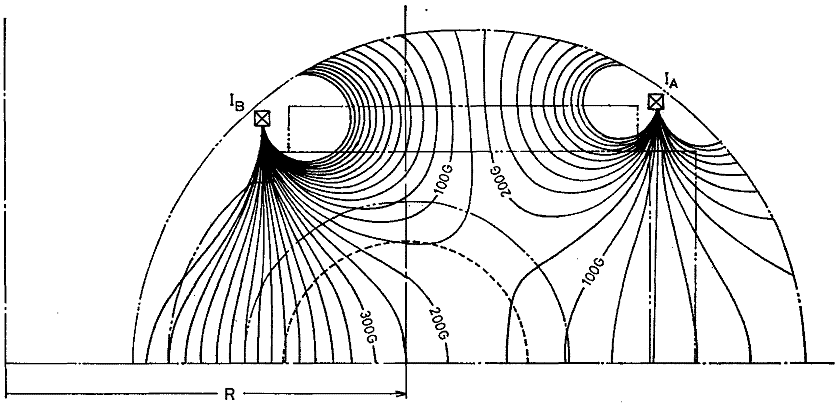

Fig. A-10. The contour lines of the vertical field in case of 4 windings. The values of I_A and I_B are the same as in Fig. A-8.

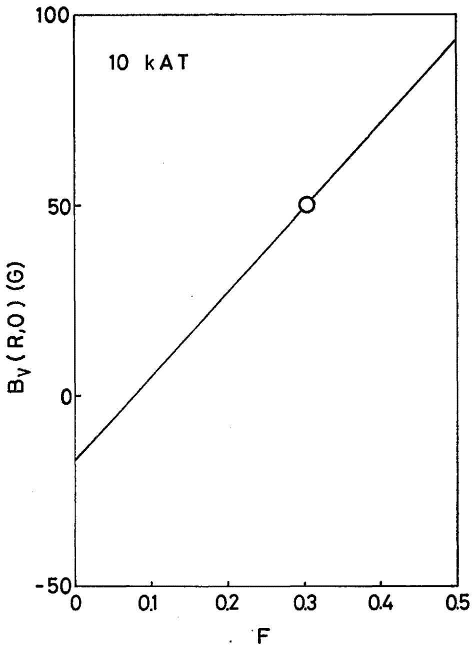

Fig. A-11. Dependence of the stray vertical field $B_V(R, 0)$ at the plasma center on the current ratio $F \equiv I_A/(I_A+I_B)$ $(I_A+I_B=5\,\mathrm{kA})$ in case of 4 windings.